1 **MECHANICAL CHARACTERISATION OF ADDITIVELY MANUFACTURED**

2 **ELASTOMERIC STRUCTURES FOR VARIABLE STRAIN RATE APPLICATIONS**

3

4

5 **Michael Robinson [a], Shwe Soe [a], Richard Johnston [b], Rhosslyn Adams [a], Benjamin**

6 **Hanna [a], Roy Burek [a,c], Graham McShane [d], Rafael Celeghini [e], Marcilio Alves [f], Peter**

7 **Theobald [a][*]**

8

9

10 [a] High Value Manufacturing Research Group, Cardiff School of Engineering, Cardiff

11 University, Wales, United Kingdom.

12 [b] Advanced Imaging of Materials (AIM) Facility, College of Engineering, Swansea University,

13 UK;

14 [c] Charles Owen, Royal Works, Croesfoel Industrial Park, Wrexham, UK.

15 [d] Department of Engineering, Trumpington Street, Cambridge University, UK.

16 [e] Centre of Engineering, Modelling and Applied Social Science (CECS), Federal University of

17 ABC (UFABC), Brazil.

18 [f] Department of Mechatronics and Mechanical Systems Engineering. Group of Solid

19 Mechanics and Structural Impact, University of São Paulo (USP), Brazil

20

21

22 *** Corresponding Author:** Dr P S Theobald, Cardiff School of Engineering, Cardiff

23 University, The Parade, Cardiff, CF24 3AA, UK.

24

25 **Abstract**

26

27 Additive manufacturing (AM) enables production of geometrically-complex elastomeric

28 structures. The elastic recovery and strain-rate dependence of these materials means they

29 are ideal for use in dynamic, repetitive mechanical loading. Their process-dependence, and

30 the frequent emergence of new AM elastomers, commonly necessitates full material

31 characterisation; however, accessing specialised equipment means this is often a time-

32 consuming and expensive process. This work presents an innovative equi-biaxial rig that

33 enables full characterisation via just a conventional material testing machine (supplementing

34 uni-axial tension and planar tension tests). Combined with stress relaxation data, this

35 provides a novel route for hyperelastic material modelling with viscoelastic components.

36 This approach was validated by recording the force-displacement and deformation histories

37 from finite element modelling a honeycomb structure. These data compared favourably to

38 experimental quasistatic and dynamic compression testing, validating this novel and

39 convenient route for characterising complex elastomeric materials. Supported by data

40 describing the potential for high build-quality production using an AM process with low

41 barriers to entry, this study should serve to encourage greater exploitation of this emerging

42 manufacturing process for fabricating elastomeric structures within industrial communities.

43

47

2

1. <u>Introduction</u>

Thermoplastic elastomers (TPEs) are co-polymeric materials that exhibit both thermoplastic and elastomeric properties, with their functional advantages meaning they are used across a broad range of applications. Tooling costs associated with traditional manufacturing methods typically constrains TPE production to high volume components only, limiting opportunities to lever a performance advantage. The emergence of additive manufacturing (AM), with unrivalled design freedom and the economic-viability of one-off production, provides new opportunities to employ TPEs in environments demanding low-volume, high-performance, or both.

Finite element analysis (FEA) simulations are well-established in the design, testing and evaluation of new and novel applications. Emerging techniques including topology optimisation and cellular lattice generation have supplemented this process, guiding designers with an over-riding objective function that prescribes the ultimate mechanical performance [1, 2]. These approaches are now being used in a series of, predominantly metal-based, weight-sensitive applications [3, 4].

The success of optimisation techniques is inherently governed by the accuracy of the material behaviour defined within the simulation. Where the analytical descriptor of a material's behaviour correlates poorly with its physical performance, the simulation will likely deliver an inaccurate solution. TPEs, which exhibit a hyper-elastic (HE) response, can be particularly challenging to characterise due to phenomena such as the Mullin's effect [5], where stress-softening occurs based on the previous level of strain experienced by the material. This results in the material's primary response (i.e. that to the first loading) differing from that of subsequent loading cycles (i.e. the stabilised response). Determining if one, or

3

74   both, of these responses are of importance to an application, is key to accurately simulating

75   HE events.

76

77   The non-linear HE response of TPE materials means they cannot be characterised by a

78   single data-point. Established constitutive models comprise a series of coefficients

79   associated with strain energy density functions capturing the variation of stress versus strain,

80   with advanced FEA software enabling the end-user to identify the model with the strongest

81   correlation to experimental data. Coefficients describing AM-produced materials typically

82   differ from traditionally manufactured equivalents [6, 7]. Whilst characterisation of AM

83   metallic structures have now been reported [8, 9], no studies quantify the rate-dependant

84   behaviour of HE AM material properties when simulating dynamic events. The technical

85   demands of such characterisation, with laboratories rarely having the requisite facilities

86   including a stand-alone equi-biaxial testing apparatus [10], risks constraining the

87   development and uptake of new TPE AM filaments and powders.

88

89   This study describes a novel experimental approach to characterise TPE materials for

90   applications experiencing strain-rates in excess of quasistatic conditions (referred to as

91   dynamic strain-rate applications), using solely a commonplace uniaxial testing machine.

92   Primary, stabilised and rate-dependant responses were captured and then fitted with an

93   appropriate HE/viscoelastic material model. Computational analysis of an exemplar TPE AM

94   structure within a dynamic strain-rate environment demonstrates both the validity of this

95   characterisation process, and the potential to enable high-performance designs.

4

2. **Materials and Methods**

Uniaxial, equi-biaxial, and planar tension data was collected to define the HE behaviour, for both primary and stabilised responses. Rate-dependant behaviour was defined by stress relaxation data. For uniaxial, equi-biaxial and planar tests, strain in the gauge area was measured using non-contact video-extensometry (iMetrum CAM028, UK). All stresses and strains are reported as nominal (i.e. engineering) data.

2.1. Materials

Table 1. Printing parameters used for this study

|			
Nozzle Diameter	0.4 mm	Extrusion Multiplier	1.4
Print speed	2000 mm/min	Layer Height	100 µm
Bed Temperature	40 °C	Active cooling	Yes
Extruder Temperature	210 °C	Infill extrusion width	125%

SOLIDWORKS (Dassault Systems, France) was used to design coupons for each test method that were manufactured in NinjaFlex (NinjaTek, US), a readily available TPE filament selected as an exemplar AM material. A fused filament fabrication printer was used (2017 Flashforge Creator Pro printer), retrofitted with high-specification extrusion control (Diabase Engineering, USA) and using processing parameters tuned to achieve a high extrusion density. Simplify3D (Simplify3D, US) was used to define print settings and slice the .STL files for printing. The common rectilinear pattern was adopted for in-filling the parts and X-ray microscopy (XRM)/microcomputed tomography (µCT) was used to confirm successful fusing of the infill extrudate. Infill was set to 100% and the extrusion settings tuned to ensure fusing of the extrudate, allowing confidence that the infill pattern would have minimal effect

5

118 on experimental results. A honeycomb was also designed and manufactured for use as a

119 case study to demonstrate the validity of this novel characterisation methodology, with part

120 quality assessed via μCT. Print orientation is shown in Figure 1.

121
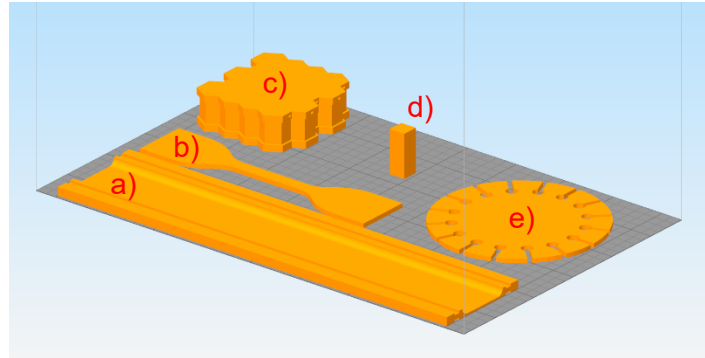
122 *Figure 1. Test part build orientations. a) Planar, b) Uniaxial, c) Honeycomb geometry, d)*

123 *Cuboid for μCT Scanning, e) Equi-biaxial*

124

125   2.2. Methods

126

127 A preliminary simulation was undertaken to establish the minimum/maximum strains

128 experienced during the loading of the honeycomb structure. This allowed identification of

129 the appropriate cycled strain during mechanical testing, used to describe the stabilised

130 response of the TPE material. A linear elastic model [11] was applied to the honeycomb

131 structure, which was compressed within ABAQUS to densification. The recorded strain was

132 approximately +/- 0.3 throughout the simulated densification of the honeycomb (to ~60% of

133 its original height). This guided the adoption of an upper strain threshold of 0.4 for

134 mechanical testing.

135 During the preliminary simulation, a mesh sensitivity study was undertaken. Varying the

136 element size from one-quarter, to twice, the wall thickness, achieved near-identical force-

137   displacement curves and little variation in predicted energies, which is consistent with other

138   studies investigating dynamic compression of cellular structures [12].

139   Five samples were manufactured for each test setup described in section 2.2.1.

140

141   *2.2.1. Mechanical Testing*

142

143   *Uniaxial (Tension) Testing*

144

145   Testing was performed using an electromechanical uniaxial testing machine (Zwick Z50,

146   Germany), following ISO 37 [13] with a reduced crosshead speed (100mm/min), to minimise

147   strain rate sensitivity. Test coupons were designed and fabricated as per tensile testing

148   specimen type 1 [13]. Investigation was performed over cyclical loading to 0.4 strain.

149

150   *Equi-Biaxial (Tension) Testing*

151

152   An equi-biaxial test apparatus was designed and built in-house, to enable multi-axial data

153   generation from a single uniaxial testing machine. Novel test coupons were designed and

154   manufactured, including 16 clamping tabs that enabled uniform application of a multi-axial

155   load, generating equi-biaxial strain in the coupon centre (Figure 2 a & b). These test

156   specimens have been shown to be appropriate for equi-biaxial testing [10], with FE analysis

157   showing little influence of geometry on the state of stress in the central gauge section.

158   Machine parameters and cycled strain were consistent with the uniaxial setup.

159
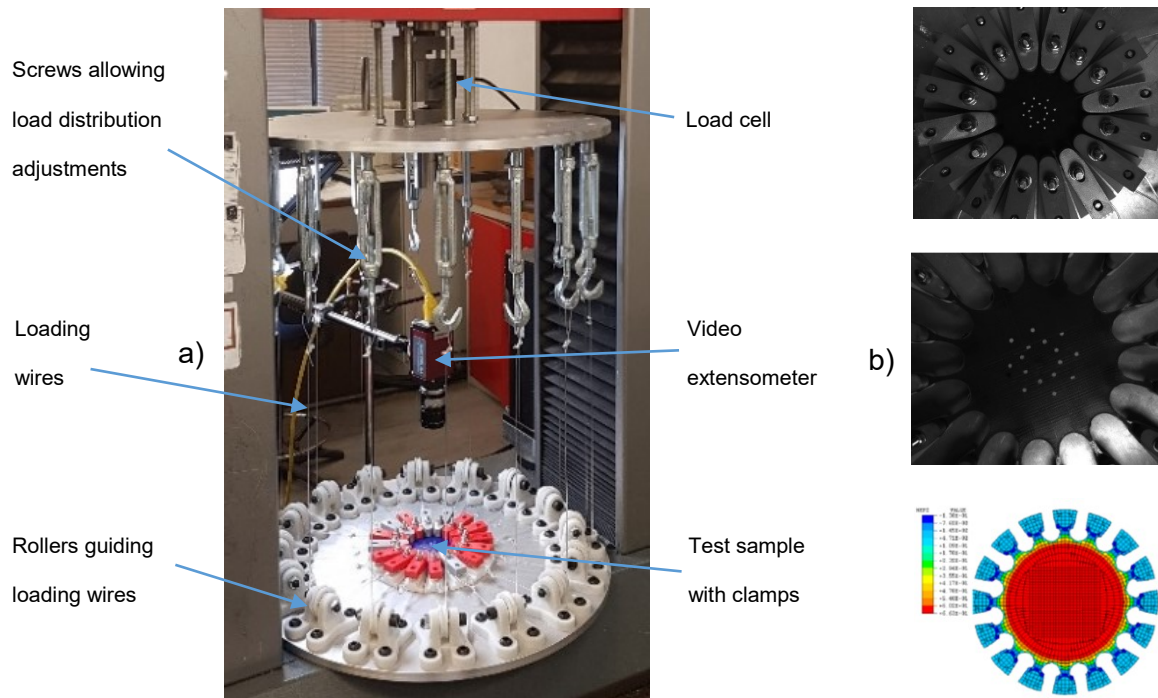
Figure 2: a) Equi-biaxial test rig, b) Stretching of Equi-biaxial sample in this study, and FEA validation of sample performed by Day, J. (reproduced from [10])

*Planar (Tension) Testing*

Shear data is valuable when modelling hyperelastic materials, which is derived from planar tension testing [14, 15]. Novel planar coupons were designed to include ridges, which improved gripping and ensured load distribution into the test gauge area (Figure 3 a & b). Machine parameters and cycled strain were again consistent with the uniaxial setup.
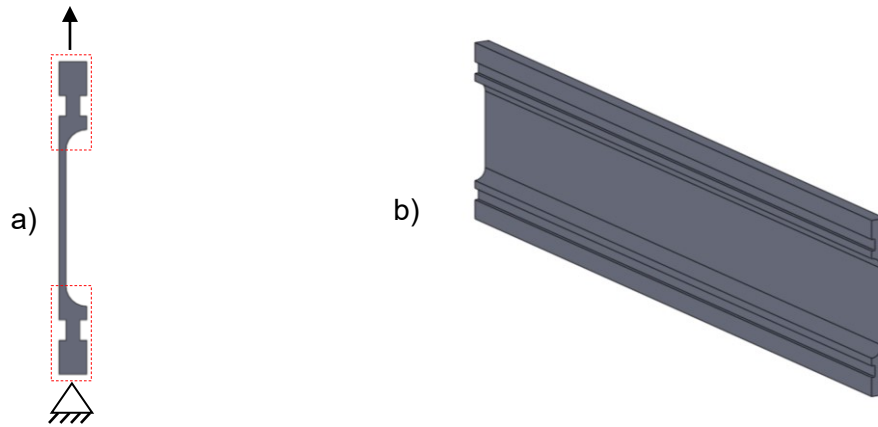
170   *Figure 3: a) Side profile highlighting ridges/added geometry on planar sample, b) 3D*

171   *visualisation of planar sample*

172

173   *Stress Relaxation Testing*

174

175   The uniaxial test geometry was used to measure stress relaxation, performed at the

176   maximum available cross-head speed (600mm/min), to a strain of 0.4 and followed by a

177   100s relaxation period. Stress relaxation experiments cannot achieve an instantaneous step

178   input and will always include an initial loading ramp, as well as inertial effects from the test

179   equipment loading. The user must compensate for these effects when analysing the data,

180   by back-calculating to a theoretical instantaneous load point, as has been performed here.

181   *Mechanical Testing of Exemplar TPE AM Honeycomb*

182

183   A NinjaFlex hexagonal honeycomb was designed and manufactured to validate the above

184   characterisation process and to demonstrate the potential of AM TPEs to produce structures

185   for high performance applications. The honeycomb structure consisted of a 4x5 unit cell,

186   with each cell having a side length of 5.8mm, 10mm height and 0.4mm wall thickness. Two

187   3mm thick solid sections were designed onto the upper and lower surfaces of the

188   honeycomb, to achieve well-defined boundary conditions. Exhaust channels (1mm

189 diameter) were designed in to the lower solid section, enabling release of air trapped within

190 the honeycomb cavities during compression and impact testing.

191

192 *Figure 4. a) sectioned view of the honeycomb part, b) indication of load direction on part*

193

194 The honeycomb structure was cyclically compressed to densification (~60% of its original

195 height) at 100mm/min (i.e. quasistatically). Industrial-strength adhesive tape (Tesa 64621)

196 was used to adhere the solid sections to the compression platens, ensuring consistent

197 boundary conditions. Dynamic testing was then performed to evaluate the relative

198 performance of the TPE AM honeycomb in a dynamic strain rate environment. A guided

199 drop tower (Instron 9250HV, US) was used to strike the honeycomb test geometry with a

200 3.53kg impactor at 1.4 m/s. This velocity ensured the honeycomb compressed to >60% of

201 its overall height. An in-line accelerometer (Kistler 8715A, Switzerland) was used to record

202 the acceleration-time pulse. Boundary conditions were defined by the lower solid section of

203 the honeycomb geometry being adhered to the anvil, and the impactor and upper solid

204 section of the honeycomb being covered with sandpaper. The impactor was released from

205 0.01m, allowing dynamic compression of the honeycomb to 60% of its original height.

206 Acceleration-time pulses were converted using standard formulae into force-displacement

207 and displacement-time data.

208

10

209   *Statistical Analysis*

210

211   Results of each test method are displayed as a mean value, with error bars representing the

212   standard deviation (SD). All testing was performed through 5 cycles/impacts, to account for

213   stress softening behaviour in the material, which decreased markedly after the second cycle

214   and was cycled a further three times to ensure a stabilised response.

215

216   *2.2.2. Computational Analysis and Validation*

217

218   ABAQUS 6.14 (Dassault Systems, France) was used first to curve-fit an appropriate material

219   model to the primary and secondary responses (for dynamic simulations the viscoelastic

220   component was added to these material models), before enabling analysis of the primary

221   and stabilised performance of an exemplar honeycomb structure. An appropriate material

222   model was then selected based on the closest correlation with the test data. Explicit

223   Dynamic Analysis was used and, in addition to any other boundary conditions/interactions

224   defined in the simulation, a global frictionless contact was defined to prevent self-penetration

225   of the honeycomb. Incompressibility was assumed (i.e. Poisson's ratio = 0.475, as this is

226   the maximum allowable in ABAQUS) and enhanced hourglass control implemented. Hyper-

227   elastic material models were fitted separately to primary and stabilised datasets. Ogden 1st

228   to 6th order, Polynomial 1st and 2nd order and Reduced Polynomial 1st to 6th order models

229   were investigated for each state. The viscoelastic component of the material model was

230   defined using normalised stress relaxation data, fitted by ABAQUS to a Prony series with

231   0.001 minimum allowable root-mean-square error. A continuum element hex-dominated

232   mesh was proliferated throughout with a seed equal to the measured average wall thickness

233   of the honeycomb (0.45 mm); however, the 3mm thick upper and lower sections of the test

11

234   part were partitioned and given a larger (default) edge seed of 0.72 mm, to reduce the

235   computational cost.

237   Due to the honeycomb walls being the same thickness as the extrusion nozzle, it was

238   expected the manufactured wall thickness would increase. Average wall thickness was

239   measured by μCT and used to update the honeycomb CAD for ABAQUS simulations. This

240   ensured identical geometry of the simulated and mechanically tested parts.

242   Quasistatic compression was computationally modelled with the honeycomb component

243   sandwiched between two rigid flat plates. The upper plate was tied to the upper solid

244   section of the honeycomb and prescribed a deflection of 0.6mm, over 1s. The lower plate

245   was fixed in space and tied to the lower honeycomb face. Viscoelastic material properties

246   were not included, whilst a mass scaling of 20 considerably reduced simulation time with

247   minimal influence on accuracy. The force-time and displacement-time histories were

248   extracted from a reference node at the centre of the upper rigid plate, enabling direct

249   comparison with mechanical testing results.

251   For simulated validation of the impact tests, the honeycomb was again sandwiched between

252   two rigid flat plates in ABAQUS. The upper plate was now assigned a 3.53kg point mass

253   and prescribed a pre-impact velocity observed during experimentation. A sliding frictional

254   coefficient of 1 was defined between the upper honeycomb surface and adjacent plate, to

255   represent a sandpaper-sandpaper contact. The lower honeycomb face was tied to the

256   bottom plate, which was fixed in space. The acceleration-time and displacement-time

257   histories were extracted from a reference node at the centre of the upper rigid plate, for

258   comparison with mechanical testing results. Acceleration-time was converted to force-time

259   using Newton's second law of motion.

2.2.3. X-ray Microscopy (XRM)/Microcomputed Tomography Scanning (μCT)

Porosity analysis was performed using a nominal cuboid structure (7.5 x 7.5 x 20 mm) manufactured from NinjaFlex and by adopting the established processing parameters. Analysis was performed via XRM using a lab-based Zeiss Xradia 520 (Carl Zeiss XRM, Pleasanton, CA, USA) X-ray Microscope, using a CCD detector system with scintillator-coupled visible light optics and tungsten transmission target. To achieve a higher resolution over the entire part height, the specimen was imaged along its 20 mm length at high resolution, using an overlap-scan and stitching procedure including five individual scans, with 15% overlap between each scan. An X-ray tube voltage of 60 kV and a tube current of 80 μA were used, with an exposure of 1000 ms and a total of 3201 projections. An objective lens giving an optical magnification of 0.4 was selected with binning set to 2, producing an isotropic voxel (3-D pixel) sizes in the range 11.862 μm. The tomograms were reconstructed from 2-D projections using a Zeiss commercial software package (XMReconstructor, Carl Zeiss), a cone-beam reconstruction algorithm based on filtered back-projection. XMReconstructor was also used to produce 2-D grey scale slices for subsequent analysis. A threshold size of 2 voxels was implemented, reflecting the boundary between pore (gas) and material of the smallest pores. Excluding data below this threshold avoids inaccurately including smaller pores during the segmentation process.

The honeycomb sample was imaged using a lab-based Nikon XT H225 microfocus X-ray microtomography (μCT) system, with a 1.3 Megapixel Varian PaxScan 2520 amorphous silicon flat panel digital X-ray imager, in reflection mode with a molybdenum target. An X-ray tube voltage of 60 kV and a tube current of 130 μA were used, with an exposure of 1000 ms and a total of 3015 projections, with a voxel (3-D pixel) size of 15.05 μm. The tomograms were reconstructed from 2-D projections using a Nikon commercial software package (CTPro version 3.0, Nikon Metrology), a cone-beam reconstruction algorithm based on

13

287   filtered back-projection. The commercial software VGStudio Max 2.1.5 was used to view the

288   reconstructed data and produce 2-D grey scale slices in TIFF format. These were imported

289   into Avizo Software (ThermoFisher Scientific, Waltham, MA, USA), where post-processing

290   including reorientation, binarization and segmentation allowed extraction of pore size and

291   volume. Honeycomb average wall thickness was measured using Vernier callipers, as well

292   as digitally via the µCT data using SOLIDWORKS (Dassault Systems, France) and used to

293   update the equivalent CAD/FEA model used for computational simulation.

294

295 **3. <u>Results</u>**

296

297   3.1. <u>Mechanical Testing</u>

298

299   The test results showed that the equi-biaxial response generated a higher stress than the

300   planar response, which was greater than the uniaxial response, at any given strain (Figure

301   6). This trend was consistent when considering both the primary and stabilised response.

302   Stress and strain for uniaxial and planar testing are presented based on the direction of the

303   loading.

304
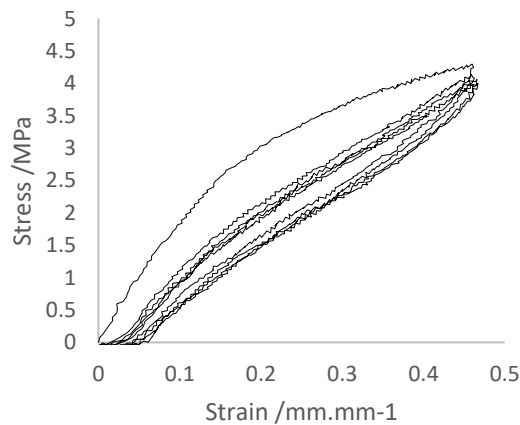
305   *Figure 5. cyclic behaviour of NinjaFlex under uniaxial loading*

306

307   *3.1.1. Primary HE response*

308

309   All datasets demonstrated non-linear behaviour typical of elastomeric materials. Uniaxial

310   testing gave an average initial modulus of 18.2MPa, when considering strains from 0 to 0.1.

311   The average initial planar modulus was 28% greater than uniaxial and the average initial

312   equi-biaxial modulus 66% greater. At a strain of 0.4, uniaxial stress was 4.11 MPa, planar

    15

313   stress was 4.66 MPa and equi-biaxial stress was 5.13MPa. The full data curves showing the

314   average mechanical test data are displayed in Figure 6.

315
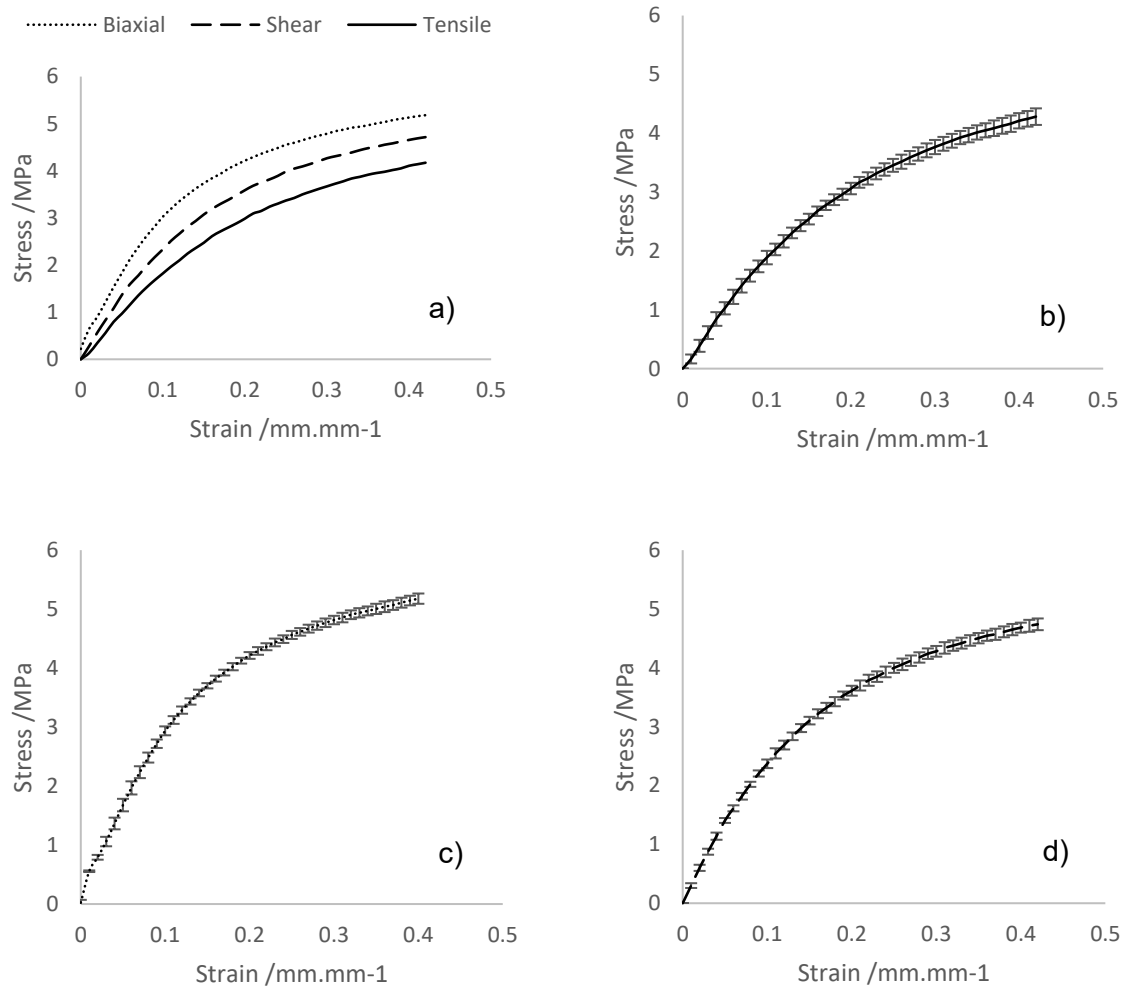
316   *Figure 6 Mechanical testing for average primary response of: a) Combined data sets, b)*

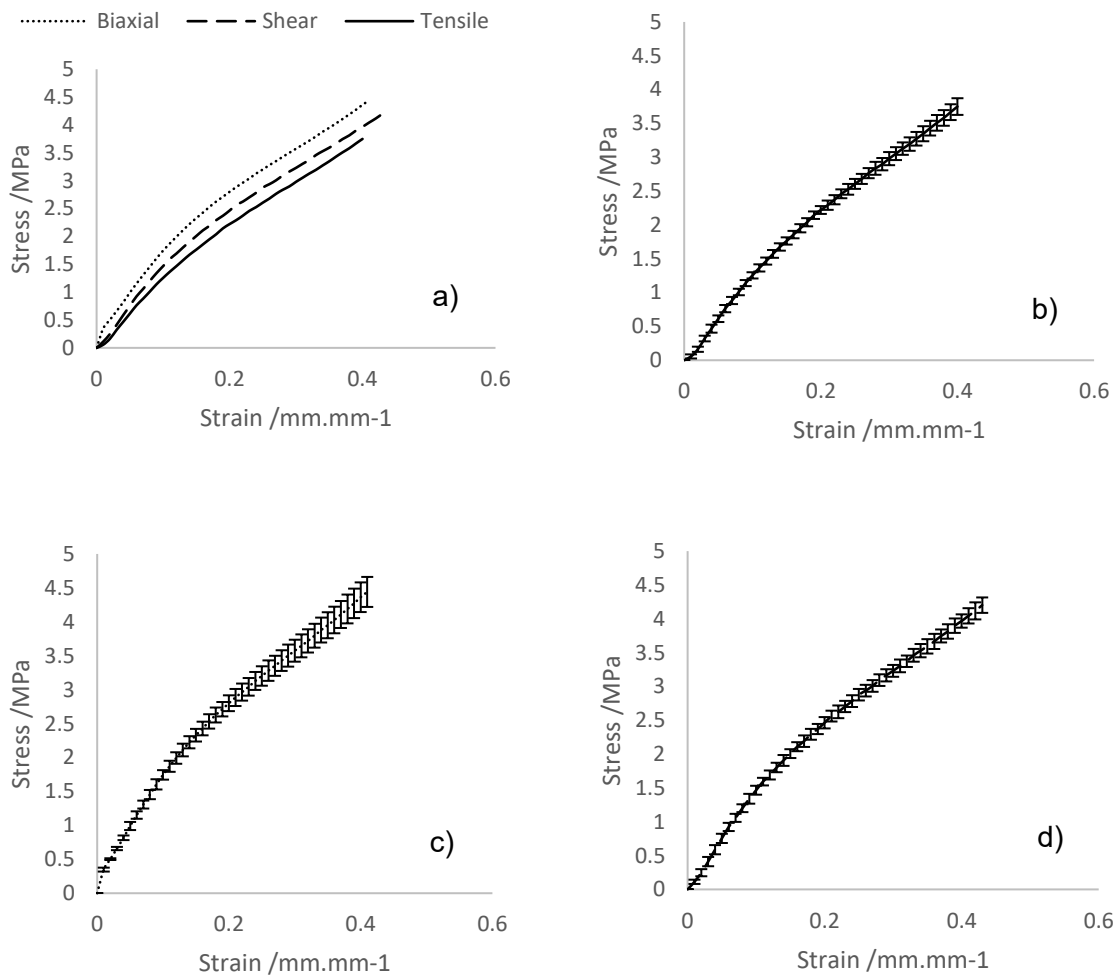317   *Uniaxial only, c) Equi-biaxial only, d) Planar only. Error bars = SD*

318

319   *3.1.2. Stabilised HE response*

320

321   The planar data trend was closer to the uniaxial, than equi-biaxial, response. Uniaxial

322   testing gave an average initial modulus of 12.5MPa, when considering strains from 0 to 0.1.

16

323   The average initial planar modulus was 18% higher than uniaxial, with the average initial

324   equi-biaxial modulus 39% higher. At a strain of 0.4, uniaxial stress was 3.75 MPa, planar

325   stress was 3.97 MPa and equi-biaxial stress was 4.36 MPa. Variance between the 5 test

326   samples for each stress state of the stabilised response was minimal, though larger than the

327   primary response data (Figure 7).

328

329   Figure 7 Mechanical testing for the average stabilised response of: a) Combined data sets,

330   b) Uniaxial only, c) Equi-biaxial only, d) Planar only. Error bars = SD

331

17

332   3.2. Curve-fitting

333

334   The ABAQUS-based curve fitting procedure for the primary and stabilised responses are

335   presented in Figure 8. The Mooney-Rivlin model provided the most appropriate fit to the

336   primary response, whilst the 2nd order Ogden model provided the best fit for the stabilised

337   response.

338
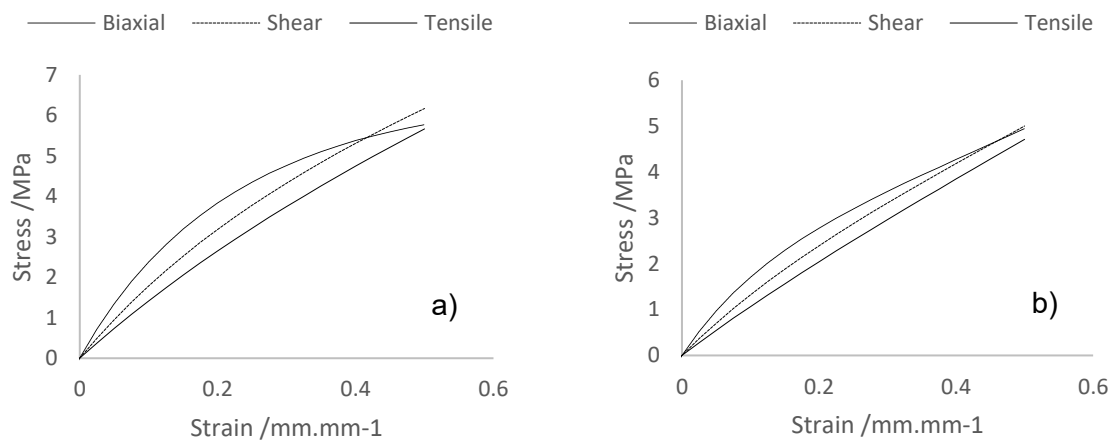
339   *Figure 8 Graphs showing combined fit for: a) Primary response, b) Stabilised response*

340

341   The coefficients for the primary and stabilised responses material models are presented in

342   Table 2 and Table 3. These models are mathematically stable, both fitting well to

343   experimental extension data and sensibly predicting the compressive behaviour, for the

344   positive and negative strain (+/- 0.3) estimated in the preliminary unit cell investigation

345   (Section 2.2.1). It should be noted that outside of the predicted strain range both models

346   become increasingly inaccurate.

347

18

348 *Table 2 Primary response – Mooney-Rivlin material model coefficients*

C10 /MPa	C01 /MPa
2.93	0.363

349

350 *Table 3 Stabilised response – 2nd order Ogden material model coefficients*

	μ1 /MPa	α1
1	12.2	1.87
2	8.41	1.19

351

352 Due to the specified low root mean square (RMS) error (0.001), the Prony series were

353 calibrated closely to the experimental data (Figure 9). Examining the experimental data

354 trend enables estimation of a long-term normalised modulus between 0.4 - 0.5. The Prony

355 coefficients that define the curve presented in Figure 9 are quantified in Table 4.

356
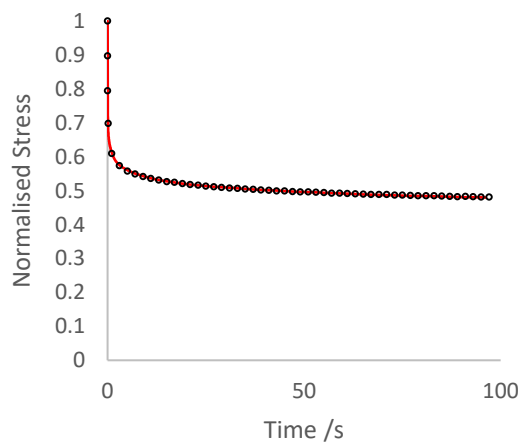
357 *Figure 9 Normalised uniaxial stress relaxation data, with Prony series curve fit*

358

359 *Table 4 Viscoelasticity Prony series*

	G /MPa	K /MPa	tau /s
1	0.196	0.0000	1.27E-03
2	0.129	0.0000	8.30E-02
3	7.67E-02	0.0000	0.894
4	6.03E-02	0.0000	6.51
5	7.10E-02	0.0000	54.6

360

361

362

363

364

365

366

367

368

369

370

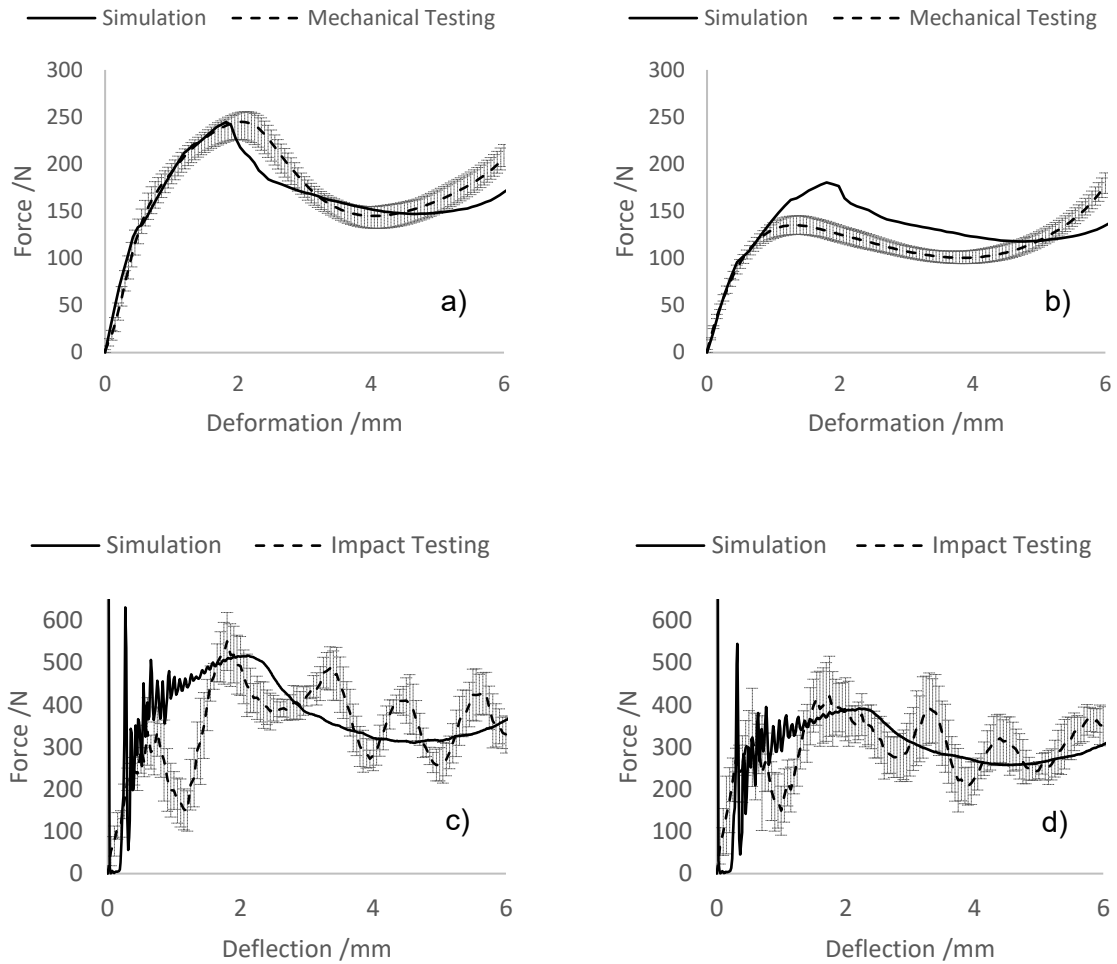371

372

373

374

375

376

377

378

379

380

381

20

382   3.3. <u>Honeycomb testing</u>

383   *Figure 10 Honeycomb validation, plotting mechanical test data alongside related simulations:*

384   *a) Primary quasistatic, b) Stabilised quasistatic, c) Primary impact, d) Stabilised impact.*

385   *Error bars = SD*

386

387   *Quasistatic Honeycomb Compression*

388

389   The plateau region varies between experimental and simulation results, influencing the

390   energy absorbed by each structure prior to densification (Table 5). For the simulated

391   primary response, agreement exists between the experimental and simulation peak forces

392   and absorbed energy; however, an increase in peak displacement of 11% was observed in

       21

393   the experimental results. The stabilised energies for the simulated and experimental results

394   were within 10% of one another.

395

396   *Table 5 Peak quasistatic forces/displacements at commencement of plateau region + energy*

397   *absorbed by structure prior to densification*

	Peak force pre-plateau /N	Displacement of peak force /mm	Energy absorbed by 6mm /J
Simulation Primary response	245	1.82	1.00
Mean Experimental Primary response	245	2.05	1.04
Simulation Stabilised response	180	1.80	0.77
Mean Experimental Stabilised response	137	1.25	0.69

398

399   At 2mm, similar s-shaped and arrow-shaped deformation patterns were observed in

400   experimental testing and simulation (Figure 11). At greater levels of compression (2 –

401   6mm), the structure begins to fold inside itself with elongated diamond-shaped patterns.

402
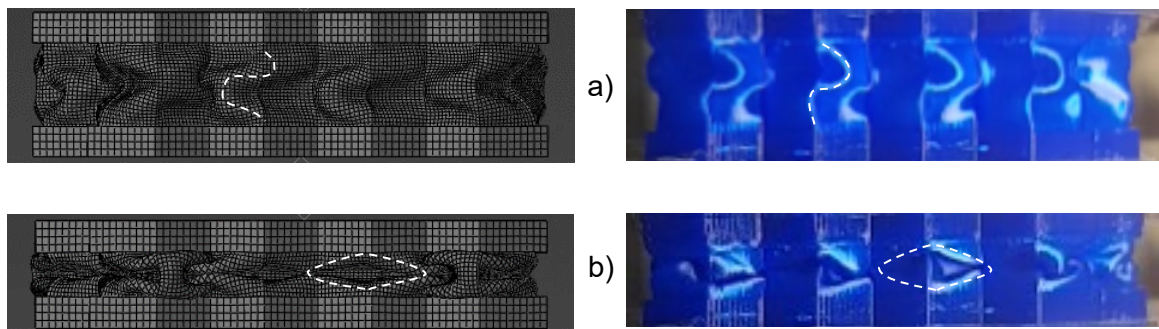
403   *Figure 11 Comparison of simulated and experimental deformation during quasistatic*

404   *compression: a) 2mm, b) 6mm. Note, simulated images have been flipped horizontally to*

405   *better highlight the similar deformation patterns.*

406   *Dynamic Compression of Honeycomb*

407

408   *Data describing the plateau regions is presented in*

409   Table 6. Experimental and simulated peak forces, displacements and energies absorbed

410   were all within 10% of one another for the dynamic primary and stabilised responses, except

411   the stabilised peak displacement, where the mechanical testing was 30% lower.

412

413   *Table 6 peak forces/displacements at commencement of plateau region + energy absorbed*

414   *by structure prior to densification dynamic*

	Peak force pre-plateau /N	*Displacement of peak force /mm*	*Energy absorbed by 6.5mm /J*
Simulation Primary response	515	1.97	2.21
Mean Experimental Primary response	550	1.80	2.10
Simulation Stabilised response	391	2.20	1.75
Mean Experimental Stabilised response	420	1.75	1.77

415

416   Distinct s-shaped deformation was identified both in experimental testing and simulation, at

417   2mm compression (Figure 12). At 6mm, the experimental testing and simulation

418   demonstrated distinctive arrow-shaped and s-shaped deformation patterns; however, the

419   simulation also had outer walls folding into the centre of the structure, similar to observations

420   during quasistatic compression (Figure 11).

421

422

23
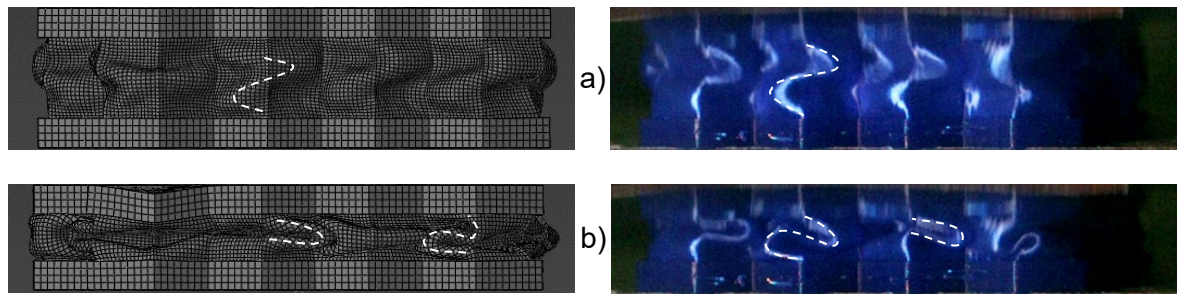
423   *Figure 12 Comparison of simulated and experimental deformation during impact: a) 2mm, b)*

424   *6mm. Note, simulated images have been flipped horizontally to better highlight the similar*
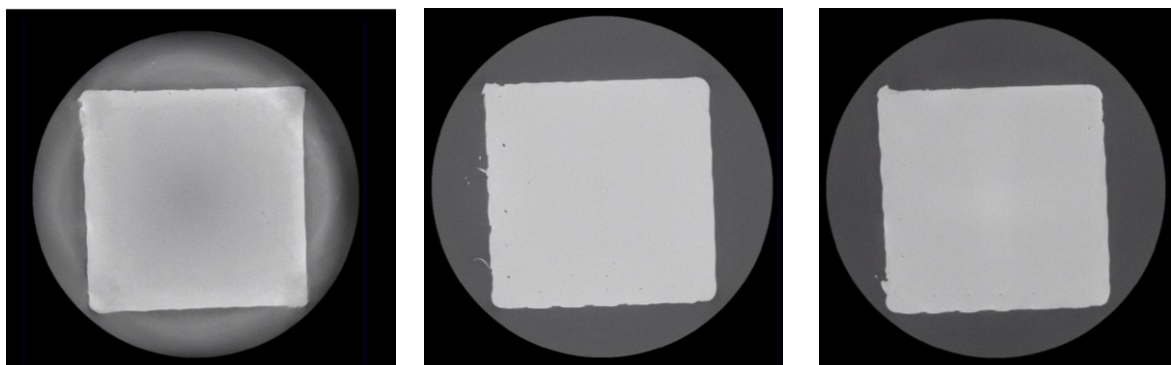
425   *deformation patterns.*

426

427   3.4. XRM/µCT Analysis

428

429   µCT scanning demonstrated that manufactured parts were largely homogenous, meaning

430   successful fusion of the extruded material (Figure 13). Additionally, the outline bounding the

431   internal rectilinear patterning was continuous, with no pores observed throughout its height.

432

433   *Figure 13 CT scanned cross-sections of cuboid geometry. Left-right: bottom, centre, top*

434

435   When analysing the pores within the scanned cuboid, those of equivalent diameter ≤2 voxels

436   (equivalent to 23.7 µm) were excluded. This was due to the potential lack of accuracy when

437   detecting pore edges of such small pores. Analysis of the remaining pores suggested the

24

438   cuboid was 99.97% dense, with an average pore size of 38 μm and a max pore size of 119

439   μm. Only ~10% of the pores were 60-119 μm, which appeared concentrated between the

440   rectilinear fill forming the cuboid centre and the outline forming the perimeter. The

441   distribution of the pores within the cuboid and the pore diameter histogram, are presented in

442   Figure 14. A one-point perspective view down the length of the cuboid illustrates the pore

443   distribution (Figure 14a). The largest pores are located at the boundary of the outline and

444   the infill pattern, in lines running the height of the cuboid.

445
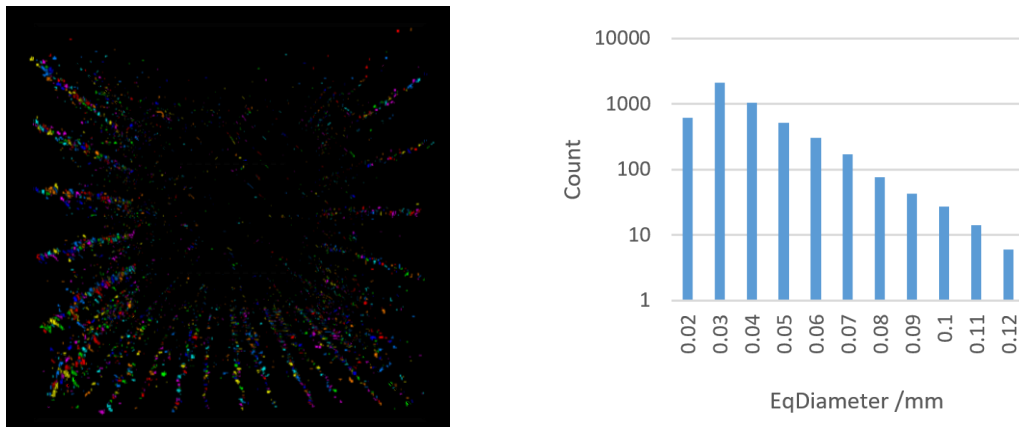
446   *Figure 14 a) 3D image of pores within the cuboid structure, with a bounding outline to show*

447   *the approximate position of the cuboid exterior, b) histogram showing the effective length of*

448   *each pore*

449

450   The μCT scan and supporting vernier measurements of the honeycomb walls gave an

451   average thickness of 0.45mm (versus 0.4mm for the CAD design) with a SD of 0.01 mm.

452   The averaged value was used to simulate a part of constant wall thickness within ABAQUS,

453   based on the minimal deviation. Some material could be observed drooping as the upper

454   surface 'bridged' over the honeycomb cell wall; however, this appeared minimal and did not

455   affect adhesion between these two features.

456

25

4. Discussion

457

458

459 The mechanical performance of TPE AM materials are known to vary with processing

460 parameters, whilst new products regularly enter the market; hence, there is an increasing

461 need to perform full characterisation, though the requisite equi-biaxial facilities remain

462 scarce.

463

464 This study has demonstrated success with a novel approach to material characterisation,

465 validated by the comparable trends achieved when experimentally and computationally

466 compressing a honeycomb structure. When applying the material models to a multi-strain

467 rate and state application, a close correlation between predicted and experimental data was

468 observed (Figure 10). The stress-softening characteristic of the Mullin's effect is evident

469 when comparing Figure 6 and Figure 7. Even at a relatively low strain (0.4), the initial

470 stiffness of the primary response is 31% higher than that of the stabilised response, and

471 15% higher stress at maximum strain. This reinforces the importance of understanding and

472 selecting the correct material response when simulating TPEs in specific applications. This

473 study has also highlighted the need to characterise multiple responses for a single material,

474 with both primary and stabilised responses being required to validate consecutive dynamic

475 compressions of a honeycomb structure (Figure 10).

476

477 Good correlation was achieved between the HE material models and experimental data

478 across both the primary ($r^2 = 0.97$) and stabilised ($r^2 = 0.99$) response.   Such strong

479 correlation provided a robust platform to investigate dynamic strain-rate applications. The

480 low RMS error requirement placed on the stress relaxation data meant that the viscoelastic

481 portion of the material model closely followed the experimental response. Consequently,

26

482 these material models accurately simulate NinjaFlex behaviour in dynamic applications of a

483 similar strain (i.e. +/-0.3).

484

485 Applying the material model to the honeycomb structure achieved strong comparability

486 between simulation and experimental data. This strong correlation validates this novel

487 method for TPE characterisation, whilst also demonstrating the potential for use in complex

488 geometries within dynamic environments. The mechanical response (Figure 10) and

489 deformation patterns (Figure 11 and Figure 12) demonstrated excellent prediction of a

490 complex HE buckling event. The quasistatic stabilised experimental and computational

491 investigations exhibited the weakest correlation. This may be caused by the residual strain

492 accumulated during stabilising loading cycles which, in combination with the fixed boundary

493 condition created by the adhesive tape, resulted in a period of tensile loading as the actuator

494 returned to the datum. Whilst this was noted and appropriately adjusted for during data

495 analysis, this additional loading regime could have triggered a unique response within the

496 material, meriting future investigation.

497 The experimental and simulated honeycombs exhibited discrepancies between their

498 deformation patterns during dynamic loading (Figure 12). Whilst the honeycomb walls

499 appeared to all form s-shaped profiles during experimental testing, a combination of s-

500 shaped and inward folding behaviour was observed in the simulated deformation patterns.

501 This appears to be focussed around the bending of the upper thick section's profile within

502 the simulation, causing inward folding to occur underneath. AM inherently results in

503 inconsistent wall thickness, minimal variation was evident and strong correlation existed

504 between the simulated and experimental stress-strain behaviour; however, such

505 manufacturing variability could still have influenced the observed deformation patterns.

506 Additionally, the buckling in the structures is a non-trivial event and, therefore, some

507 deviation in deformation patterns was expected between the simulated and experimental

508 behaviour. Structural response can also be influenced by contact behaviour; however, this

27

509 study investigated pre-densification behaviour and, when running these simulations with a

510 general frictional contact (as opposed to frictionless), minimal change in stress-strain

511 behaviour was observed.

512

513 This study assumed linear viscoelasticity and, whilst the use of non-linear viscoelastic

514 models may help to further fine-tune the prediction of varying strain rate behaviour, this

515 comes at a substantial computational time cost. In the light of this drawback, the close

516 correlation of predicted behaviour presented here serves to justify the assumption of linear

517 viscoelasticity. In the light of mainstream adoption due to low machine costing, fused

518 filament fabrication (FFF) is considered by many to be a rudimentary/entry level technique.

519 The potential of FFF to produce high quality components is, however, demonstrated here,

520 with an excellent cuboid part density of 99.97%. This exceeds previously reported densities

521 achieved via Selective Laser Sintering (SLS) TPE components (~95%) [16] and is

522 comparable to injection moulded parts. Accounting for 94% of the cumulative pore volume,

523 the largest voids (70-119µm) are technically challenging to eliminate in FFF builds and

524 existed between the rectilinear fill and bounding outline of the cuboid. During tuning of

525 processing parameters, attempts to reduce these voids included the use of concentric

526 (instead of rectilinear) fill, increasing extrusion multiplier, and increasing overlap between the

527 inner rectilinear fill and bounding outline. These methods introduced their own issues such

528 as the concentric fill generating significant voids in the centre of the part, whilst increasing

529 overlap/extrusion multiplier resulted in distortion of printing parts. It should be noted that the

530 threshold size of 20µm was selected to ensure the pores within the entirety of the cuboid

531 could be captured in a single scan. Whilst this provides a suitable indicator of the porosity of

532 the part (as the pores circa 70-110µm accounted for 94% of the measured pore volume),

533 this has the potential to filter out smaller pores that could have an undetermined influence on

534 material behaviour.

535   It is known that the layer-by-layer AM build process produces component anisotropy, with

536   this behaviour frequently noted in the literature perpendicular to the layer deposition [17-19].

537   This behaviour is highly dependent on manufacturing build quality as this logically effects the

538   inter-layer bonding. As complex printed components can be exposed to different strain

539   states, potential exists for loadings to be applied parallel and perpendicular to inter-layer

540   bonding, even if the overall structure is only under compressive loading. Due to the lack of

541   notable voids, similar deformation patterns/mechanical responses and good correlation

542   between stress-strain behaviour of the honeycomb structure, no further investigation of

543   anisotropy was performed in this study. AM manufacture also means that thin some

544   geometric features comprise only a single track of extruded filament (i.e. as per the entire

545   honeycomb structure), creating the potential for a different mechanical response than parts

546   with infill patterning (e.g. test parts used to characterise NinjaFlex). This risk was mitigated

547   against by using process parameters that achieved minimal voids in the recti-linear fill

548   pattern, with good correlation evident between the simulated honeycomb response (using

549   infill patterning characterisation) and the mechanical testing (of single extrudate honeycomb

550   print).

5. <u>Conclusions</u>

This study has achieved a greater understanding of the behaviour of TPE AM materials, enabling more effective exploitation of this emerging technology. A novel approach to efficiently and robustly characterise TPE materials has been presented. The importance of considering strain-softening has also been demonstrated, along with the potential to design and analyse AM structures for high performance applications. Highlighted findings include:

- Multi-state strain data to define a material model has been acquired using a standard uni-axial testing machine.

- A material model has been fitted to the TPE test data, including viscoelastic effects. This model is then successfully validated through its application to a case study of a traditional hexagonal honeycomb at varying strain rate.

- The level to which the TPE material was strained had significant effects on subsequent straining of the material, an important consideration when developing material models for applications involving multiple cycling events.

- When dynamically compressed, the viscoelastic properties significantly affect the recorded forces, demonstrating a significant degree of strain-rate dependence. These strain-rate effects carried over to the manufactured parts, resulting in a significant increase in recorded force when dynamically compressed, compared to quasistatic compression.

- FFF has been used to fabricate TPU components of high homogeneity (material density of 99.97%), with expected manufacturing considerations spreading material at the extruder nozzle, resulting in an increased wall thickness.

30

576 **6. <u>Acknowledgements</u>**

577

583

31

7. <u>Bibliography</u>

1. Huang, X., et al., *Topology optimization of microstructures of cellular materials and composites for macrostructures.* Computational Materials Science, 2013. **67**: p. 397-407.

2. Coelho, P.G., et al., *A hierarchical model for concurrent material and topology optimisation of three-dimensional structures.* Structural and Multidisciplinary Optimization, 2008. **35**(2): p. 107-115.

3. Brackett, D., I. Ashcroft, and R. Hague. *Topology optimization for additive manufacturing*. in *Proceedings of the solid freeform fabrication symposium, Austin, TX*. 2011. S.

4. Leary, M., et al., *Optimal topology for additive manufacture: a method for enabling additive manufacture of support-free optimal structures.* Materials & Design, 2014. **63**: p. 678-690.

5. Mullins, L., *Softening of Rubber by Deformation.* Rubber Chemistry and Technology, 1969. **42**(1): p. 339-362.

6. Mower, T.M. and M.J. Long, *Mechanical behavior of additive manufactured, powder-bed laser-fused materials.* Materials Science and Engineering: A, 2016. **651**: p. 198-213.

7. Gorsse, S., et al., *Additive manufacturing of metals: a brief review of the characteristic microstructures and properties of steels, Ti-6Al-4V and high-entropy alloys.* Science and Technology of Advanced Materials, 2017. **18**(1): p. 584-610.

8. Wadley, H.N.G., N.A. Fleck, and A.G. Evans, *Fabrication and structural performance of periodic cellular metal sandwich structures.* Composites Science and Technology, 2003. **63**(16): p. 2331-2343.

609 9. Ajdari, A., H. Nayeb-Hashemi, and A. Vaziri, *Dynamic crushing and energy*

610   *absorption of regular, irregular and functionally graded cellular structures.*

611   International Journal of Solids and Structures, 2011. **48**(3-4): p. 506-516.

612 10. Day, J. and K. Miller, *Equibiaxial Stretching of Elastomeric Sheets, An Analytical*

613   *Verification of an Experimental Technique*, in *ABAQUS users' conference*. 2000:

614   Newport, RI. p. 205-220.

615 11. Ninjatek, *NinjaFlex® 3D Printing Filament*, in *Ninjatek Technical Specifications*,

616   Ninjatek, Editor. 2016, Ninjatek.

617 12. Abueidda, D.W., et al., *Mechanical properties of 3D printed polymeric cellular*

618   *materials with triply periodic minimal surface architectures.* Materials & Design, 2017.

619   **122**: p. 255-267.

620 13. BSI, *BS ISO 37:2017 - Rubber, vulcanized or thermoplastic — Determination of*

621   *tensile stress-strain properties*. 2017, BSI.

622 14. Treloar, L.R.G., *The physics of rubber elasticity*. 1975: Oxford University Press, USA.

623 15. Bergstrom, J.S., *Mechanics of solid polymers: theory and computational modeling*.

624   2015: William Andrew.

625 16. Dadbakhsh, S., et al. *Effect of powder size and shape on the SLS processability and*

626   *mechanical properties of a TPU elastomer*. in *Physics Procedia*. 2016. Elsevier.

627 17. Frazier, W.E., *Metal Additive Manufacturing: A Review.* Journal of Materials

628   Engineering and Performance, 2014. **23**(6): p. 1917-1928.

629 18. Soe, S.P., et al., *Mechanical characterisation of Duraform® Flex for FEA hyperelastic*

630   *material modelling.* Polymer Testing, 2014. **34**: p. 103-112.

631 19. Ahn, S.-H., et al., *Anisotropic material properties of fused deposition modeling ABS.*

632   Rapid prototyping journal, 2002. **8**(4): p. 248-257.

633